Ocean Engineering
December 2023, Volume 289 Pages 116154 (9p.)
https://doi.org/10.1016/j.oceaneng.2023.116154
https://archimer.ifremer.fr/doc/00860/97144/

An empirical model to predict elongation of polyamide mooring lines

François Michel [1], Davies Peter [2, *]

[1] Consultant for Bureau Veritas, France
[2] IFREMER Centre Bretagne, France

* Corresponding author : Peter Davies, email address : peter.davies@ifremer.fr

Abstract :

Polyamide mooring lines are being proposed for station-keeping of floating wind turbines in shallow water. However, their mechanical behaviour is quite different to that of the polyester fibre ropes used for deep water offshore oil & gas platform moorings. This paper presents an empirical model which can predict the specific strain response of a polyamide 6 mooring line under stochastic loading. Particular attention is given to the non-linear load-strain behaviour, hysteresis, and the influence of loading history. The identification of the model, using 12 stochastic tests performed on wet 3-strand polyamide sub-rope samples, is described. This model reproduces the specific features of the response of fully wetted PA ropes well, with reasonable accuracy and, for the extreme (maximum and minimum) values it provides a much better prediction than the linear “dynamic stiffness” model. This new model can be integrated in the time domain processing of a suitable mooring analysis software.

Highlights

► Development of a model framework to predict mooring line elongation. ► Identification of model parameters for polyamide. ► Application to the case of representative stochastic load sequences. ► Excellent correlation between model predictions and tests.

Keywords : Polyamide, Non-linearity, Dynamic stiffness, Stochastic, Floating wind

1 Introduction

Synthetic fibre ropes have been used in marine applications for over 50 years, progressively replacing the natural fibres such as hemp, which had been standard equipment on naval vessels for over five centuries. Polymer fibre yarns can be produced at rates of kilometres per minute to tight dimensional tolerances, and modern rope-making technology assembles them in continuous twisted and braided structures. There are two main categories of fibres; high performance fibres such as high modulus polyethylene (HMPE) and aramids, and more commodity products such as polyesters (PET) which represent the majority of current world production, polyolefins (polyethylene and polypropylene), and nylons (polyamide 6 and 6.6). While most of the commodity fibres are destined for the textile industry there is an increasing market for polyester and polyamide 6 in mooring lines [1] where low weight, high specific properties and low cost provide an attractive alternative to steel wire and chain.

1.1 Synthetic fibre mooring lines for floating wind

In order to optimize the dimensioning of station-keeping equipment it is essential to be able to characterize its response over a range of loading conditions. This is a challenge, as the single stiffness approach which suffices for steel is no longer applicable and different values of stiffness are needed to represent different situations. Extensive work on PET fibre ropes during the

development of their use as deep water mooring lines for offshore oil & gas led to a set of property data and standard test procedures [2, 3]. However, for floating offshore wind turbines in shallow or intermediate waters, PET moorings are too stiff. The preferred material for these depths at present is polyamide 6 [4-6], which shows significantly different properties to PET [7]. It is therefore necessary to develop and validate stiffness models for PA fibre ropes in order to predict their elongation in service. There have been some attempts to do this recently. For example, Pham et al developed a dynamic stiffness model, which included both mean tension and amplitude parameters in a mooring line analysis applied to a floating wind demonstrator [8]. Chevillotte [9], then Civier et al [10], described a more complex model developed within the POLYAMOOR project, based on a spring and dashpot model proposed previously by Flory et al. [11]. West et al examined the influence of the stiffness models in DNV and API Guidelines and concluded that the model choice has a significant influence on nacelle accelerations and surge response, particularly for large sea states [12].

Several recent papers have examined the mooring of floating wind turbines. Xu et al [13] looked at seven different mooring concepts for 50-meter water depth, including a taut synthetic line. Its stiffness was modelled using the approach developed for polyester within the SYROPE JIP [14], with a linear dynamic stiffness dependence on mean tension. The authors conclude that further fatigue analysis is needed to validate the concepts. Pillai et al [15] discuss mooring of a 15 MW floating wind turbine using polyester and the novel Exeter tether, an elastomer-based system. The synthetic solutions significantly reduce peak loads compared to chain mooring systems and also limited excursions. Verde and Lages also present a study of mooring of a 15 MW turbine and compare polyester and nylon directly [16]. They show a reduction in peak loads of 44% for the nylon but at the expense of larger rotations and displacements. Model tests on a point absorber also show the strong influence of axial stiffness and pre-tension on peak loads [17].

The objective of the present paper is to propose an alternative empirical approach to stiffness modelling; this provides an improved representation of the non-linear load-strain response compared to the traditional dynamic stiffness approach. The model identification is based on realistic load spectra rather than the more usual sinusoidal loading sequences.

The fibre rope lines of a station-keeping system in service are fully submerged, and subject to a random amplitude tension cycling, around a slowly varying (a time frame of several hours or days) mean tension, that is dictated by the setting of the system and the overall (mean) forces induced by metocean elements and system operations.

The process is assumed to be stationary, over durations of around one to six hours, and includes a “wave frequency” (WF) part, a “low frequency” (LF) part (around natural periods of the system), and possibly higher frequencies, induced by turbine operation for example. The response of ropes to this process is the subject of this paper. The response to the variations of mean tension, and to non-stationary conditions (e.g. the effect of sudden - squall - winds), is not addressed here.

1.2 Dynamic stiffness

For Polyester ropes for station keeping, tests under cyclic action (constant or random amplitude) show an almost linear response (tension versus elongation), that can be characterised [18] by a “Dynamic stiffness”. This dynamic stiffness is then obtained from tests with constant amplitude cycling [2, 3]. For Polyester it is solely dependent on - and increasing quite linearly with - the mean tension. Similar observations were made with other materials, particularly high modulus fibres [19].

Other effects (cycling amplitude, frequency …) were observed in early work but were shown to have thermal origins, induced by hysteretic heating under certain test conditions (dry rope and cycling at a constant - relatively large - range). They disappear when the rope is wet or immersed, and do not exist under - realistic - stochastic loading [20].

1.3 Polyamide rope behaviour

To date, PA has been used in hawsers offshore, in applications such as Single Point Moorings. These are typically changed every one to two years and this product does not correspond to the requirements for mooring a permanent floating wind turbine. A detailed study on PA6 ropes was performed within the OHP (Offshore Hawser Properties) JIP (2007 – 2013), with considerable testing performed, at IFREMER and IFPEN, on samples of new and aged hawsers for tanker mooring.

Additional studies highlighted the sensitivity of polyamide fibres to moisture [21], well known from tests on bulk polyamide [22], indicating that rope properties should be measured on wet samples. The dynamic stiffness of PA6 ropes was found, as for other materials, to be principally dependent on mean tension (and almost proportional to it for a fully wetted rope), but also dependant on cycling amplitude. This indeed raises a dilemma for the evaluation of the extreme tensions in a mooring analysis. With random amplitude cycling, it appears in tests as a load history dependence.

In addition, at large amplitudes and/or low minimum tension, the response is not linear, showing (on plots of tension versus elongation) a curvature and some hysteresis, as illustrated in Figure 1 below.

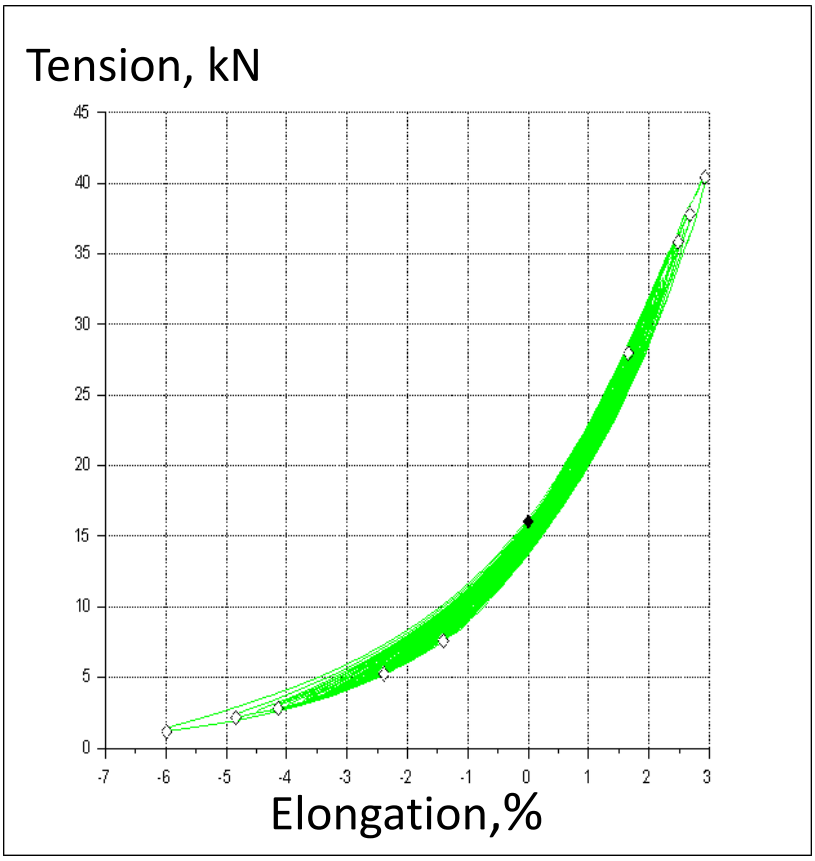

Figure 1. Plot of Tension (kN) versus elongation (% - see 3.1), typical polyamide 6 rope (test 4G)

Point at [Xmean,Fmean]: (◆), *points at F1 & F2:* (◇) *– see 3.2*

Modelling these aspects in mooring analysis software cannot be achieved with a set of stiffness values nor characteristics, as currently available for PET: a specific predictive model is needed. It has to be a time domain model, which can be integrated in the time domain processing of lines in mooring software packages.

A first outline of a model was built based on OHP test data. The model was subsequently developed further based on stochastic tests performed at Ifremer during both the POLYAMOOR and MONAMOOR projects, (see Acknowledgements section for further details of these projects).

2 Materials and Test methods

The materials described here are PA6 fibre ropes intended for station keeping, manufactured by Bexco (Belgium) for the POLYAMOOR and MONAMOOR projects. Twisted 3-strand subropes, 15mm diameter for the two projects, were tested on a 300 kN servo-hydraulic test frame. The corresponding wet break loads were measured to be 70 kN. Figure 2 shows a 15mm diameter specimen on the test frame; 6-meter long samples were terminated with eye splices, which fitted over 100mm diameter test pins to attach the sample to the test frame. Samples were immersed in tap water for 4 hours without load before testing and wetted continuously during testing. Elongations were measured in the central rope section, between the splice ends over a free length of around 2 meters, with wire displacement transducers attached to the rope. Load, piston displacement, central section strain (typically over a length of around 1.2 meters between the splices) and temperature values were measured continuously during the tests at a sampling frequency of 10 Hz.

Figure 2. Sample on test frame and detail of wetting

2.1 Testing sequences

The testing sequences from which the present model was developed are 1 hour random amplitude time series, extracted from the results of simulations of the permanent mooring of a FOWT (with a semi-submersible floater), and scaled to subrope size. In the POLYAMOOR project six tests were performed, each with a different signal, obtained from different lines and/or seed in the analyses for two different storm conditions (extreme and milder). Some constant amplitude and bi-harmonic tests were also performed.

In the MONAMOOR project, four tests were performed, all based on the same signal (POLYAMOOR PS4), but with different scaling factors, to complement those of POLYAMOOR, on the effect of mean tension.

In addition, two runs were performed with a stochastic load signal from the OHP project, that was also derived from a simulation (a tandem offloading), and that combines a WF part with a dominating LF part.

A summary of these tests is given in Table 1 below.

Test	Mean Tension (kN)	Tension Range (kN)	Objective
PS	14.7 to 16.3	10.6 to 34.9	6 tests
4N	15.3	24.0	Repeat of PS4
4R	9.2	14.4	Fmean effect
4H	19.9	31.2	Fmean effect
4G	16.1	38.4	Higher range
H32	15.0	10.5	LF dominated / small range
H32B	15.0	20.9	LF dominated

Table 1. Summary of stochastic loading tests performed

The tension time series, including typical single band (WF) and dual band response processes, can be deemed representative for different types of floaters. The PS signals do not have a HF content, but bi-harmonic tests (WF+HF) indicated the response to small embedded HF cycle is similar to that

of WF in bi-harmonic (LF+WF) tests, and so will be equally well captured by the model (see also 3.6.3 note a). Besides, with maximum tensions and tension ranges up to about 55% of the rope break strength, minimum tensions down to about 3%, and mean tensions up to about 30%, these tests cover a wide range of tension (see also below).

2.2 Stabilisation

In a typical test run for cyclic actions, be it constant or random amplitude, these actions are applied around a specified mean tension, and the plot of elongation versus time shows a progressive stabilisation of the mean elongation, with a sign (creep or recovery) and magnitude both depending on previous time history. In the conditions of a station-keeping system once installed and for some time after, and by the assumption of a stationary state noted above, the mean tension during a sea-state is constant and the mean elongation can also be considered as fully stabilised.

In the present tests, a pre-cycling (bedding-in) sequence at the mean tension, 100 cycles at a constant amplitude lower than the peak loads in the subsequent signal, was applied before each run, to meet this condition. A verification of the stability of mean elongation (also of mean tension) was made, using a 3 parameter least square fit to a log of time function as detailed in [2]. See Figure 3 for illustration.

This indicated that, principally for tests 4R to 4H (probably due to previous test history) the mean elongation was not well stabilised. A correction of the elongation was made for these tests, (see 3.2.1 below).

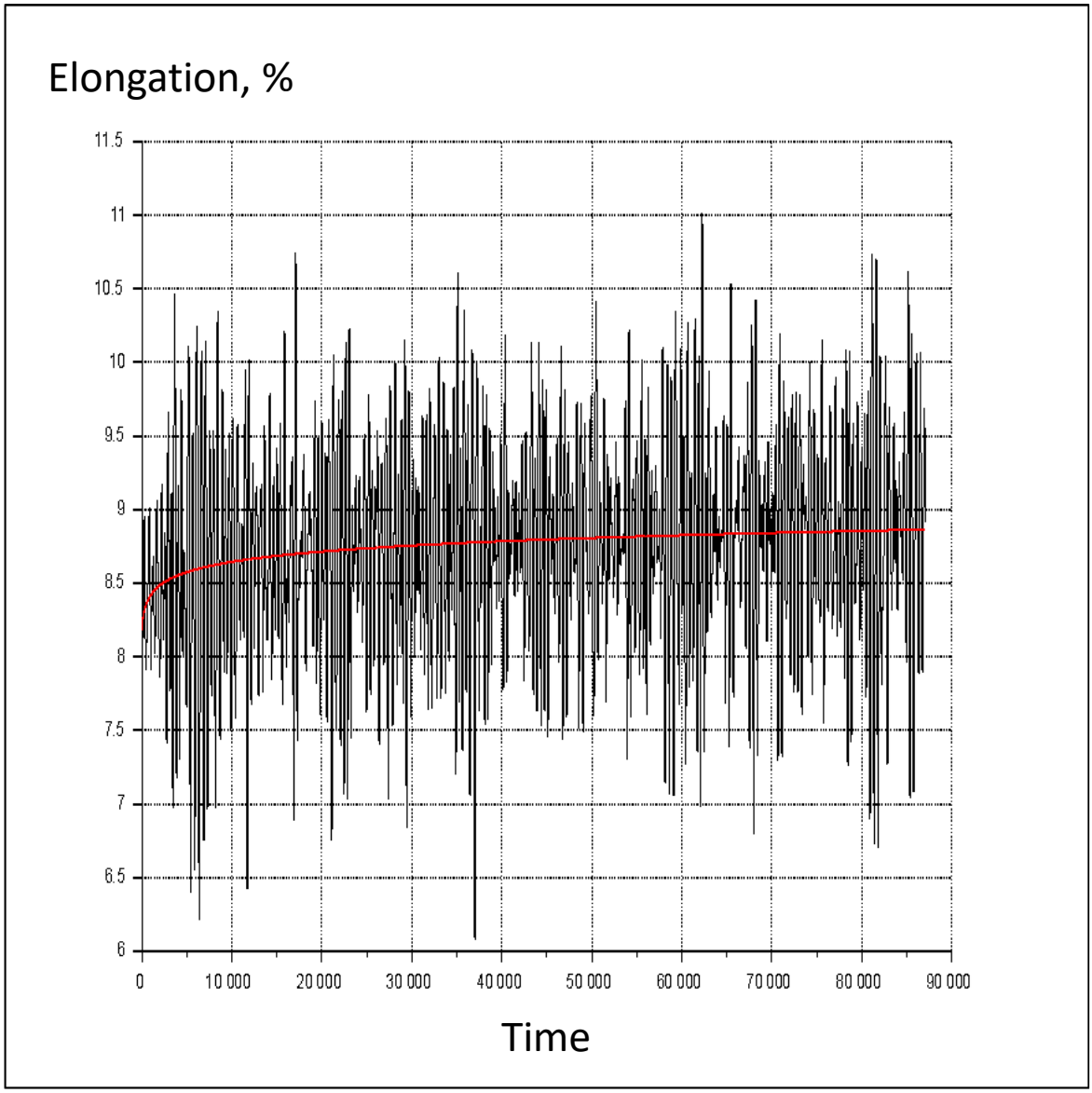

Figure 3. Verification of strain stability.

Elongation versus time (black) test 4N, Xm fit to log of time function (red)

2.3 Results

Test results fully confirm the observations made on curvature and hysteresis, as noted in 1.3 above, and their dependence on the amplitude of tension of each test. In particular, the smaller amplitude tests (such as PS1 and H32) evidence that, for small amplitudes the response tends to a linear one. Other aspects are discussed in the section 3 below.

2.4 Data sampling

The POLYAMOOR tests were run at the same speed as the source signal. The MONAMOOR tests were run at a reduced speed (by a 2.5 factor), to avoid the difficulties in control and extensometer systems found during the POLYAMOOR tests, which were caused by the high compliance of PA ropes. A small (high frequency) noise was observed however, principally in the elongation (X) signal. For compatibility with the Rain Flow Counting (RFC) process used in the model (see section 3.2.2), the signals were smoothed by least square spline fitting then resampled so as to get the same number of points as for the previous tests. This eliminates most of the noise.

3 Model description

3.1 Definitions

The symbols and units used in model development and throughout the present document are the following:

F	Instantaneous Tension at point of interest (kN)
Fmean (or Fm)	Mean line tension (kN)
Ff	Normalised tension Ff = F / Fm - 1
F1	Previously observed lowest minimum tension (kN), at a given time step,
F2	Previously observed highest maximum tension (kN), at a given time step,
X	Instantaneous Rope elongation, in % of the length corresponding to a tension Fm (see 3.2.1-1 below)
X1 & X2	Elongations at F1 & F2
v12	v12 = v2 - v1 for a variable v.

3.2 Outline, assumptions

The proposed model is an empirical model, with assumptions and formulations based on the observations from tests. The objective is to reproduce, in the context of a mooring analysis, both the mean stiffness and the specific features of the response of PA ropes, as noted above:

- Curvature,
- Hysteresis,
- Load history dependence.

3.2.1 Assumptions

The following assumptions were made, as further detailed below:

1. The length of a rope segment under tension is written as:

$$L(F) = L_0 (1 + Xs/100) \cdot (1 + Xd/100) \quad (1)$$

in which:

- L_0 is the initial length of the rope segment,
- Xs is the quasi-static elongation under the mean tension Fm (not addressed in the present work; see 1.1 above).

  In tests Xs is the observed mean elongation. When the test is not well stabilised (see 2.2 above), Xs at each time step is taken from the above-mentioned log-of-time function.
- Xd is the "dynamic" elongation resulting from tension variations around Fm (X in the present document***).***

2. The model provides the rope elongation versus time, as a function of rope tension, and previous loading history, when tensions are normalised by the mean tension Fmean (see 3.3).
3. The elongation of the rope is a "pseudo-elastic" elongation, and does not include any time dependent term. (see 3.4).
4. Concerning the dependence on load history, the model is based on the decomposition of the tension signal, by the technique of rain flow counting (RFC), (see below).
5. Besides, it is assumed that the response at any time is a function of only the previously observed minimum & maximum (normalised) tensions F_1 & F_2.

3.2.2 Rain Flow Counting Process

Rain Flow Counting is, for over 5 decades, the industry standard for the analysis in the time domain of materials subject to random amplitude cycling, e.g. for cycle counting (fatigue analysis), or in the case of hysteretic (elastoplastic) response. A very straightforward formulation of the RFC process

was proposed in [23].With RFC, the tension signal is broken down into a number of closed cycles, embedded in an envelope formed by the residual (a set of half-cycles) of the RFC process.

A first step in this process is the identification of successive local maxima and minima of the signal (the “turning points” in [23]), from which the sequences of the previously observed minimum & maximum tensions F1 and F2 can be extracted.

Note: as illustrated in figure 4, the tension signal is then subdivided in segments with constant F1 & F2, except at their very end (for the transition to the next F1 or F2).

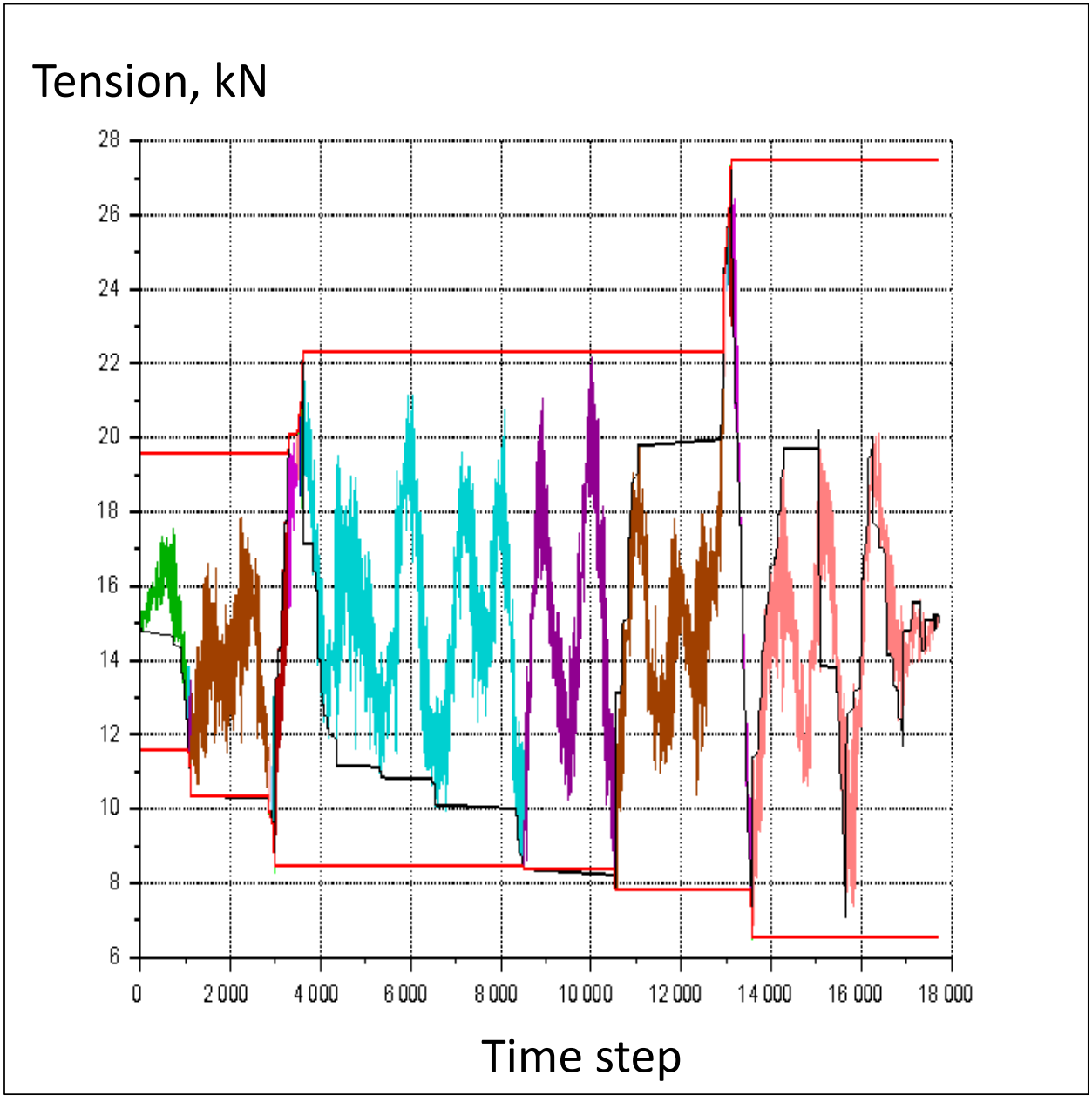

Figure 4. Test H32B: Tension versus time step

RFC embedded (closed) cycles (color by segment) and residual (black); F1 & F2 (red)

For the data points within each extracted (full or half) cycle, the response is then predicted by:

- a model of elongation cycles in each segment, i.e. when the tension is varying within the interval [F1, F2], with parameters depending, by assumption, (only) on F1 and F2 ,
- a downward and an upward envelope, when F goes outside the interval] F1, F2 [.

Note: These relations are written here as Elongation X versus the Tension F, but as the response is pseudo-elastic (i.e. not including a visco-elastic contribution), with all turning points of F and X coinciding in time, it could equally be written as Tension versus Elongation (see also 3.6.3 b).

3.2.3 Identification of parameters

From observations of the test records, a model was first assumed; then the parameters of the model were obtained by a combination of least square fits on selected sets of the elongation signals, and trial-and-error on the selection of functions, all in an iterative process. The resulting model is presented in the following section.

Processing was carried out with specific routines, written using SCILAB [24]. For computing efficiency, the use of the vectorial capabilities of SCILAB was maximised (each time series has about 35000 data points), but keeping in mind the objective of a predictive time domain model.

3.3 Mean Tension

The constant amplitude tests (not shown here) confirmed the earlier finding of the OHP project, that the dynamic stiffness is proportional to mean tension; thus that the dynamic elongation is a function of the normalised tension, F / Fmean.

During model development, it appeared that the elongation can be also represented using function(s) of this normalised tension. This is consistent with the finding above.

For stochastic tests, this was verified by comparison of the elongations between tests 4N (repeat of PS4), 4H, and 4R (same signal, scaled up and down). These show a close fit (see figure 5), with however some variability in a spindle shape, probably an effect of the small variations of (normalised) tension signal over the 3 tests.

PS4 was found to deviate from the above measurements (likely an effect of incomplete stabilisation of the three MS tests), and also shows more scatter due to inaccuracies in PS tests (see 2.3 above); however, no effect of the different cycling period could be identified.

Besides, model parameters b and ah (see 3.5 below) for the above 3 tests show some scatter (reflecting the observed variability between the measured signals on the test bench) but no trend on Fmean other than the normalisation.

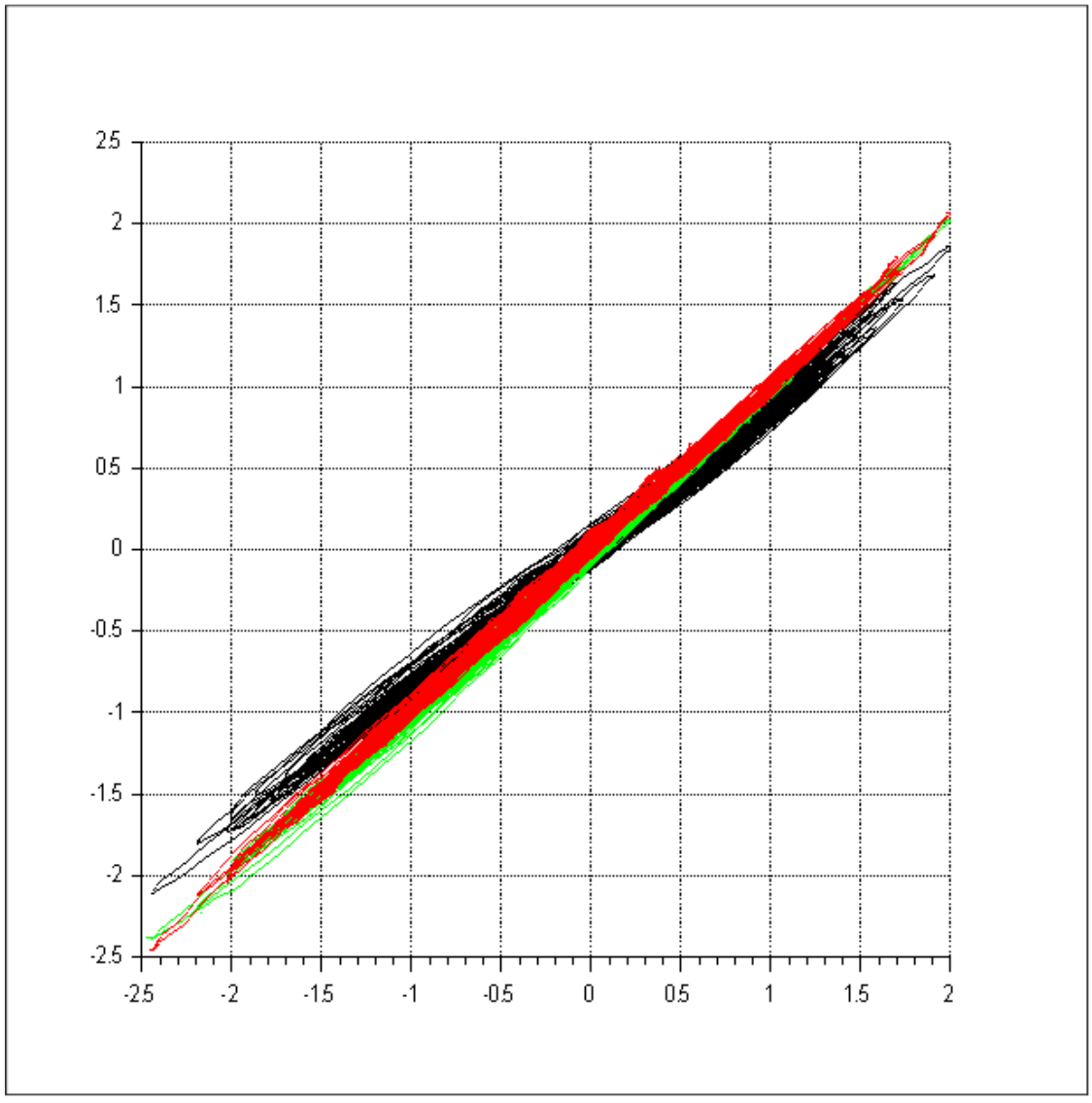

Figure 5. X-X plot. Elongation versus elongation of test 4N:

4R (green), 4H (red) & PS4 (black)

3.4 Time dependence

A close look at signals around the maxima and minima of F and X indicates a small shift between those of F and those of X. Together with the observed hysteresis, this could reveal either a creep and relaxation contribution around Fmean (the creep or relaxation under Fmean is not addressed here) or a visco-elastic contribution.

However, for the first term, correlation plots showed no correlation between $FP = \int (F - F_{mean}) \, . \, dt$, the driving term for this, and X; nor between FP and XD, the residual of the model (see 4.1 below).

A visco-elastic term could be an elongation function of the time derivate of F, or a (more classical) viscous term on tension, function of the time derivate of X. A weak correlation is observed, but no consistent term over test duration, nor between different tests, could be derived.

In any case, the difference dX = Xmax – X(Fmax) around the maxima of tension and elongation (same for minima) appears small (less than 0.5% of the maximum range of the test), and this effect will be neglected in the present model.

3.5 Envelope

In a tension versus elongation (F v X) plot, it is observed that the points at successive (first occurrence of) F_1 or F_2 form envelopes of the overall signal. Besides, the envelopes from all tests are found to collapse to a single curve, with some scatter however, when:

- The elongation is taken with respect to the mean length of rope, following equation (1) above,
- The tension is normalised by the rope mean tension Fmean, as noted above.

Results from MONAMOOR tests (see figure 6 below) are quite well in line with those of POLYAMOOR, except those of 4N, 4R, and 4H, which are close together (see 3.3 above). They deviate somewhat from other results (as also observed for cycle model parameters, it appears that the correction on mean elongation (see 3.2.1) is not sufficient to obtain the fully stabilised conditions as achieved in other tests).

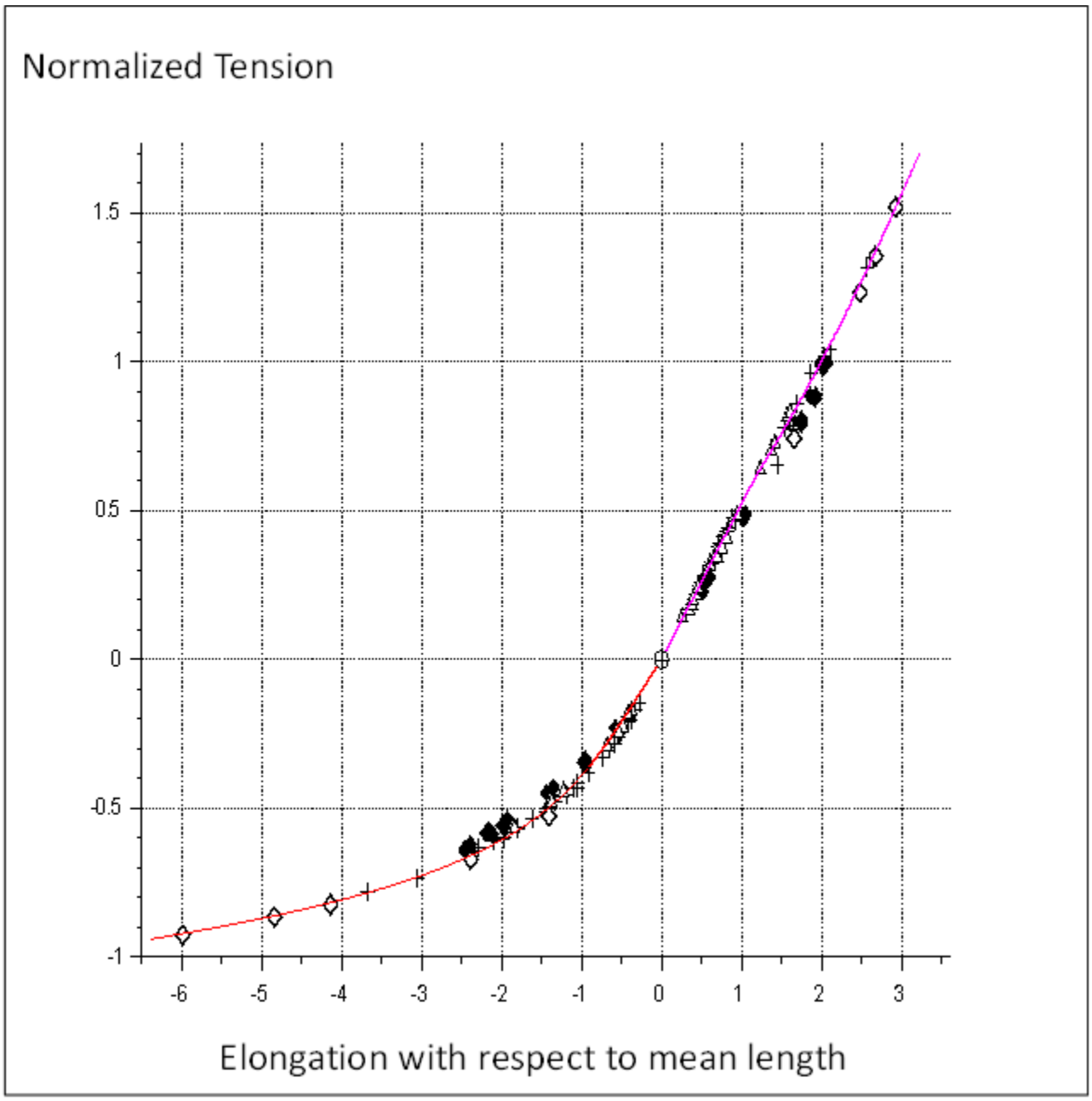

Figure 6. Envelopes of normalised tension Ff versus elongation.

Data points : PS (+) , 4 N,R, H (◆), 4G (◊) , H32 &H32b (△) & Fit (red)

The envelopes are then determined by non-linear least square fitting of X versus Ff, with selected data (fully stabilised MONAMOOR tests 4G, H32 and H32B), and the following functions:

- For the upward envelope:

$$X = ua + ub \cdot Ff^{uc} \qquad (2a)$$

with $X = ud \cdot Ff$ for small Ff (below about 0.62) (2b)

where:

ua, ub, uc, and ud are constants (see Table 2 in 3.6.4 below).

- For the downward envelope:

$$X = da \cdot |Ff| + db \cdot |Ff|^{dc} \quad (3)$$

where:

da, db, and dc are constants (see Table 2 in 3.6.4 below).

Note: At Ff = - 1, i.e. at a zero tension, the downward envelope extrapolates to about -8% elongation, whatever Fm. This may not be realistic for low mean tensions. However, no correction is applied, as it is expected that a correction for such a near-slack condition would have little effect on the prediction of the overall response by a mooring analysis.

3.6 Cycles

3.6.1 F- X relation (curvature)

In order to account for the curvature observed in the plots of tension F versus elongation X and omitting hysteresis, the F-X relation is taken, in each segment, as a (shifted) exponential function. This is written as:

$$F + F0 = (Fk + F0) \cdot \exp[(Xe - Xk) / b] \quad (4)$$

where:

- F0 defines the shift of the (theoretical) asymptote,
- b is a scale parameter,
- Xk is the elongation at an (arbitrary) value Fk of the tension,
- Xe is the elastic elongation, neglecting hysteresis.

Taking F = F2 and Fk = F1, this can be written as:

$$F2 + F0 = (F1 + F0) \cdot \exp[(X2 - X1) / b] \quad (5)$$

The end points (at F1 & F2) being on the envelope (by definition), this equation expresses a constraint between b and F0: b is taken as the independent parameter, then:

$$F0 = \{ F2 - F1 \cdot \exp[(X2 - X1) / b] \} / \{ \exp[(X2 - X1) / b] - 1 \} \quad (6)$$

Equation (4) can also be written as:

$$Xe = X1 + b \cdot \ln [(F + F0) / (F1 + F0)] \quad (7)$$

Thus: $Xe = a + b \cdot z$ with $z = \ln (F + F0)$ (7a)

i.e. a linear relation between Xe and z.

3.6.2 Hysteresis

In order to account for the hysteresis observed in the plots of tension F versus elongation X (i.e. ascending and descending half cycle load paths that are not coinciding), the elongation X is written:

$$X = Xe + Xh \quad (8)$$

Following the observation in earlier work (OHP bi-harmonic superposition tests), it is assumed that, when plotted as z versus x and shifted to a common origin, all (up and down) half-cycles in one segment follow the same function. Indeed, in stochastic tests, some scatter is observed (see figure 7). This scatter happens predominantly at the start of half-cycles and in small (embedded) cycles.

Xh is thus taken as: $| Xh - xs | = b \cdot H (| z - zs |)$ (9)

in which xs and zs are the values of x and z at the starting point of a half-cycle.

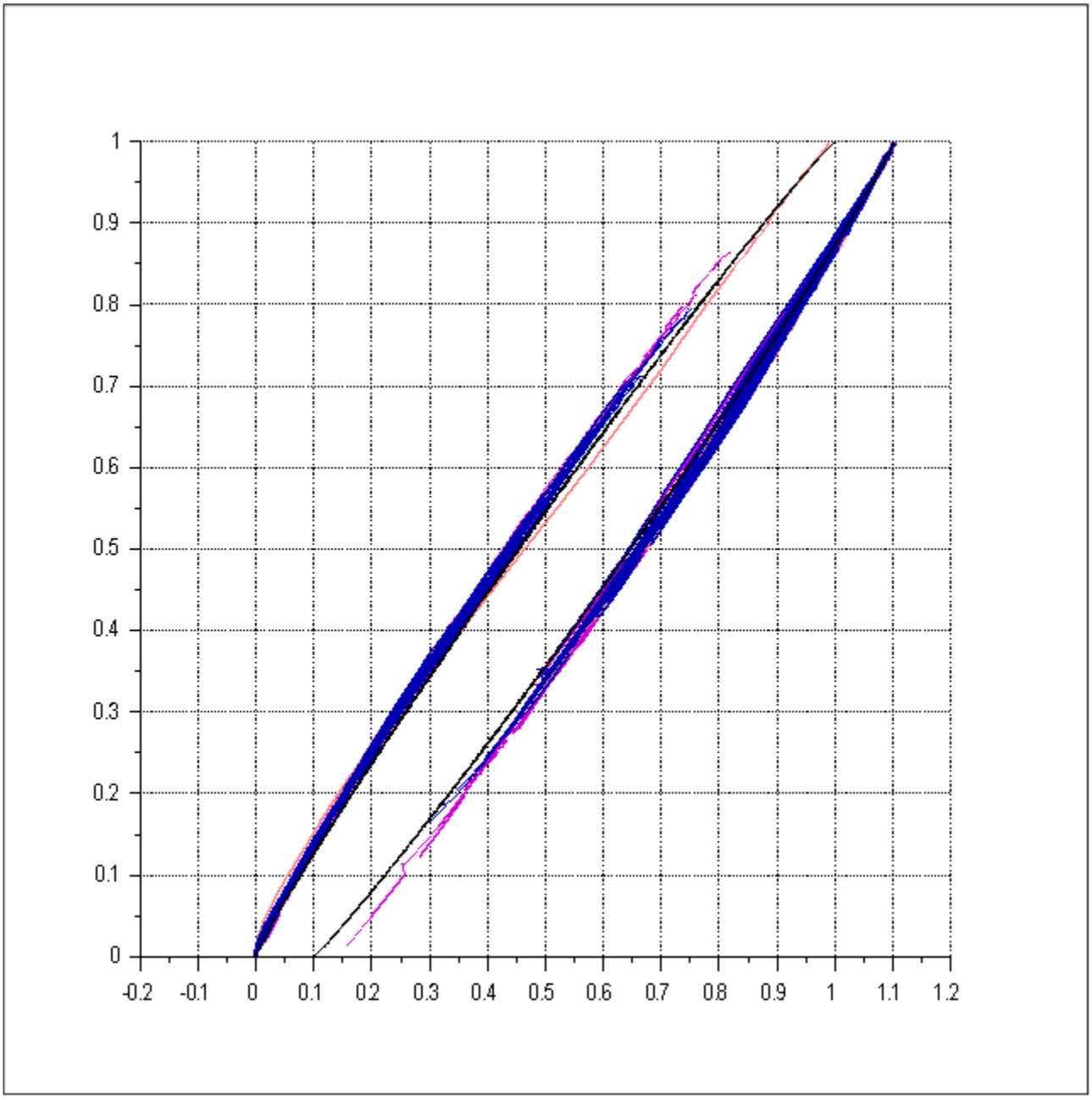

Figure 7: Test 4G: Shifted and normalised half cycles zr versus xr

Up and down (shifted) Data (color by segments) & model (black)

This is written in a non-dimensional form as:

$$xr = r(zr)$$

with: $zr = | z - zs | / Z12$, and $xr = | x - xs | / X12$,

where X12 and Z12 are the range of X and Z between the tensions F1 and F2:

$$X12 = X2 - X1 \qquad Z12 = X12 / b$$

Hr is taken as a modified quadratic function:

$$xr = Hr(zr) = hp \cdot [\, 4\, zr \cdot (1 - zr)\,]^{ph} \qquad (10)$$

in which:

- ah is the (non-dimensional) amplitude of hysteresis (the value at zr=0.5)
- ph is an exponent.

Other more complex functions (for Xe and Xh) could lead to a better fit, but consistent values of related additional constants could not be found.

3.6.3 Notes:

(a) The hysteresis is small but should not be neglected as, following equation (9), it results in the higher “stiffness” of small cycles, when embedded in larger ones, such as WF in dominating LF (see e.g. H32B in figure 9) or HF in WF (observed in POLYAMOOR bi-harmonic tests).

b) In order to write as Tension versus Elongation, the above equations can be easily inverted. However, for Hr^{-1} (that is diverging at near zero h), and hp being small, one should use:

$$zr = Hr(xr\ ,\ -\ hp)$$

3.6.4 Derivation of model parameters

The model parameters (b, ah & ph) are assumed to be functions of (normalised) F1 and F2.

However, F1 and F2 (normalised or not) are, by their nature, strongly correlated in the database of tests, the same for their combinations (mean and range), and for the resulting elongations:

The range of elongation X12 (itself a function of (normalised) F1 & F2 - see 3.4 above) - appears as the most pertinent variable.

The model parameters are then obtained by a (non-linear) least square fit of data in each segment (omitting too short segments) of each test, but a direct 3 parameter fit on shifted half cycles does not work well. Thus, the fit is performed on a reconstructed signal (see 4.1 below) in each segment.

Omitting the first segments in each test, which are affected by the (constant amplitude) pre-cycling (see 2.2), the results indicate for b that X12 / b (the factor in F0 equation) is increasing (about) linearly

with X12. Those for ah indicate that the dimensional hysteresis ah · X12 is increasing (about) quadratically with X12.

This is written as:

- $X12 / b = ax + bx \cdot X12$ (11a)

with b= 1.0 for small Ff2 (below about 0.38) (11b)

where:

ax and bx are constants.

- $hp \cdot X12 = ah \cdot X12 + bh \cdot X12^2$ (12)

where:

ah and bh are constants.

Note: at small X12 (below available data points) the parameter b is taken to get convergence to a linear response when the tension range tends to zero (see 2.3 above). So, the model will correctly cover low amplitude situations, such as the milder sea-states under operating conditions.

Related constants are obtained by linear regression on data from the tests 4G, H32B and H32 (also PS1 to 3 - smaller ranges - for ah). The power term ph is taken as a constant.

Table 2 shows values of model constants, for the subrope tested here.

			Unit
	F	Rope tension	kN
	X	Rope elongation (see 3.2.1)	% of length under Fm noted below "%e"
XED	da	-2.37	%e
	db	-5.52	%e
	dc	4.58	-
XEU	ua	-1.14	%e
	ub	3.14	%e
	uc	0.622	-
	ud	1.92	%e
X12/b	ax	0.266	-
	bx	0.295	$\%e^{-1}$
hp	ah	3.21E-02	-
	bh	1.73E-03	$\%e^{-1}$
Hr	ph	0.7	-

Table 2. Values of model constants for PA6 sub-rope

4 Reconstruction and comparison with measurements

The model has been evaluated by comparing predictions with data from the stochastic time series.

4.1 Elongation versus time

With the equations in 3.5 and 3.6 above, the parameters for all segments can be evaluated, then the elongation signal can be reconstructed. This reconstructed signal appears to be very close to the observed signal (see example in figure 8), in almost all cases, except for:

> Significant variations at the start (first 2 to 10 minutes, depending on the signal): this is likely to be an effect of repeated cycling between 2 fixed levels during pre-cycling, that is not addressed by the present model. Besides, for the first segment, the result is not valid, being affected by the

(arbitrary) assumptions that have to be made on X(1) and hp. This initial period is omitted in the following.

> Step changes of the mean residual XD (observed X - model X) over segments, being probably an effect of the forcing of end points to the envelope equations.

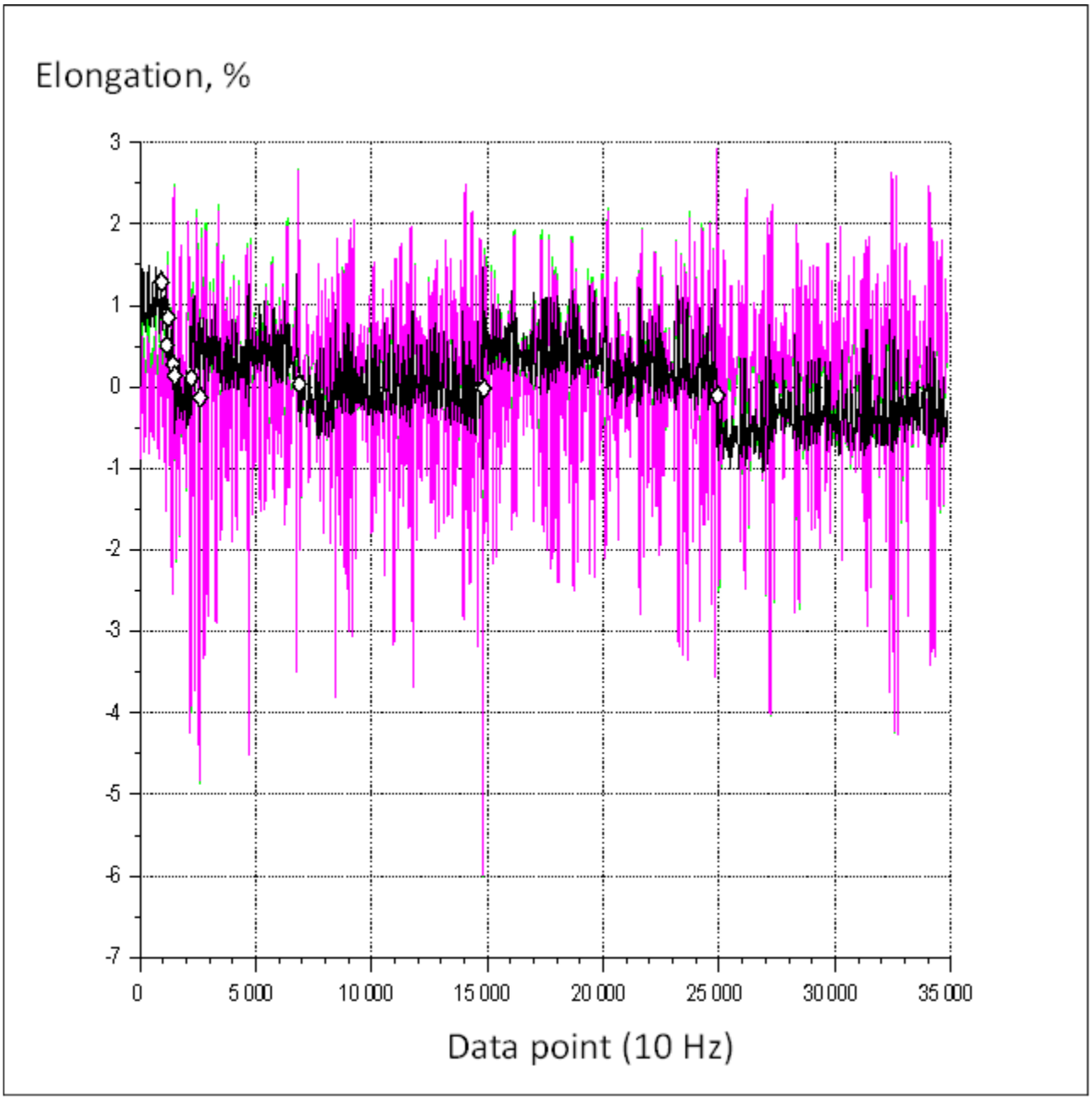

(a)

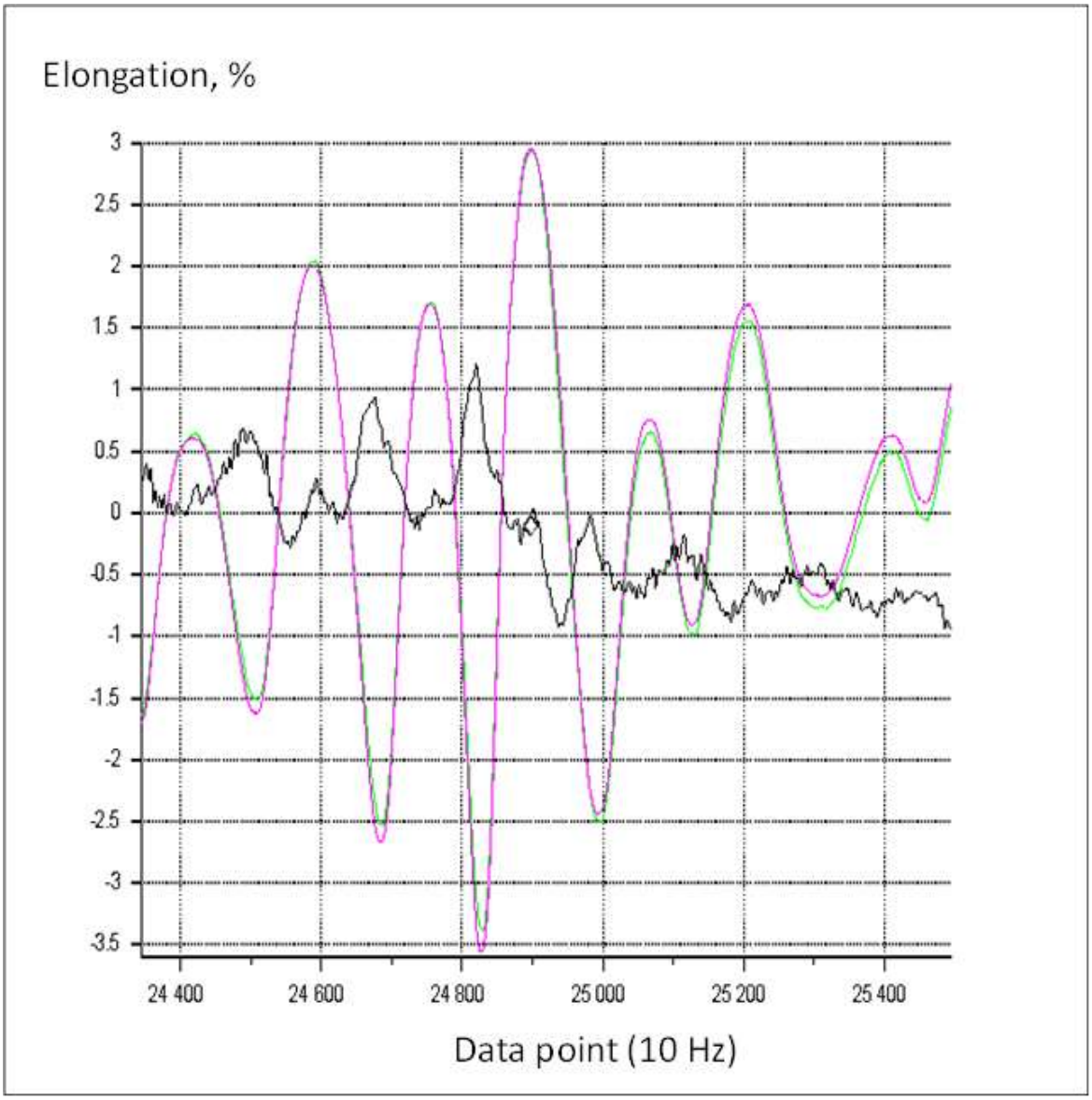

(b)

Figure 8. Test 4G: Elongation versus time step

a): Full test b): Zoom

Observed (green) ; model (pink) ; residual x5 (black)

4.2 Model error

The model error (model X - observed X) is expressed below, for each test, as a percentage of the observed range of elongation between the points at maximum and minimum tensions in that test, that is varying from 1.4 (PS1) to 8.9 (4G) percent elongation.

For tests 4G, H32B, H32 and PS tests, and except for a few outliers:

> The standard deviation of the residual is about 1% (or less) of the observed range, and the (absolute value) of mean error does not exceed about 1 % of the range.

> The maximum error is generally less than 4.5 % of the range,

> The errors at the points at maximum and minimum tensions (i.e. the predicted max and min elongations) are lower (generally below 2.5%). This is much lower than the error with the linear "dynamic stiffness" model (about 10% to 20% of the range of elongation, see also Figure 9 below).

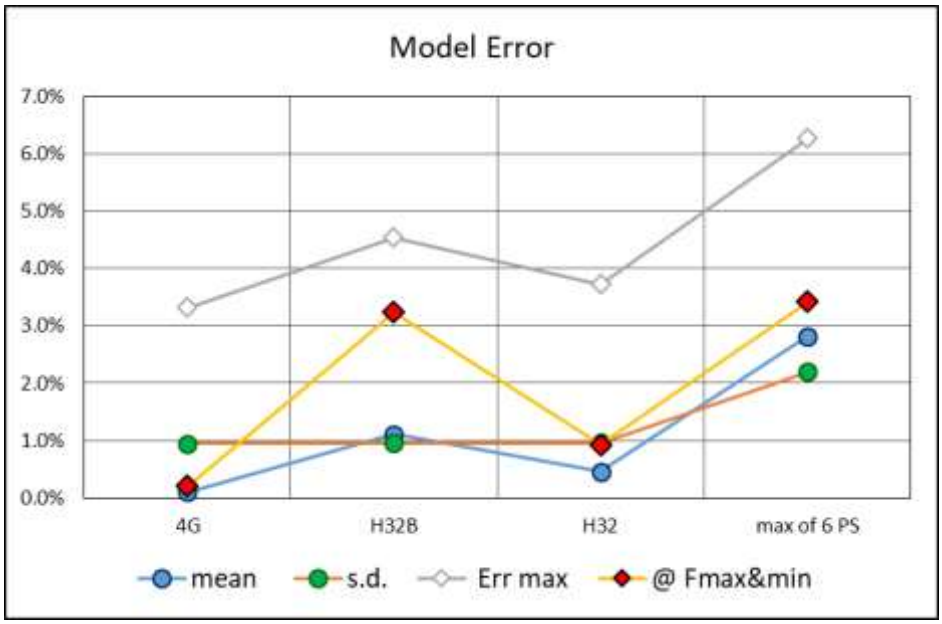

Figure 9. Model error (on elongation) versus tests

(in % of the maximum range in each test)

4.3 Tension versus Elongation

Overall, a good fit is observed on plots of tension versus elongation for all tests (see examples in figure 10, other tests show similar trends).

> Discrepancies appear mainly related to the variability of observed elongations at the successive F1 & F2 values, with respect to envelope equations, and to the effect on (large) cycles resulting from the forcing of end points to the envelope.

> For large half-cycles (e.g. H32B in figure 10), some effect of the variability of curvature with respect to that given by parameter b is observed, while the hysteresis appears quite properly estimated.

Comparing the hysteresis work $W = \int (F - F_{mean}) \cdot dX$ between model and observed elongations shows a similar order of magnitude, with a ratio around 1 for PS

tests, somewhat lower for the others (0.5 to 0.85), but this underestimate is not deemed significant, as the hysteresis is small, and unlikely to provide any significant contribution to the damping of the global system.

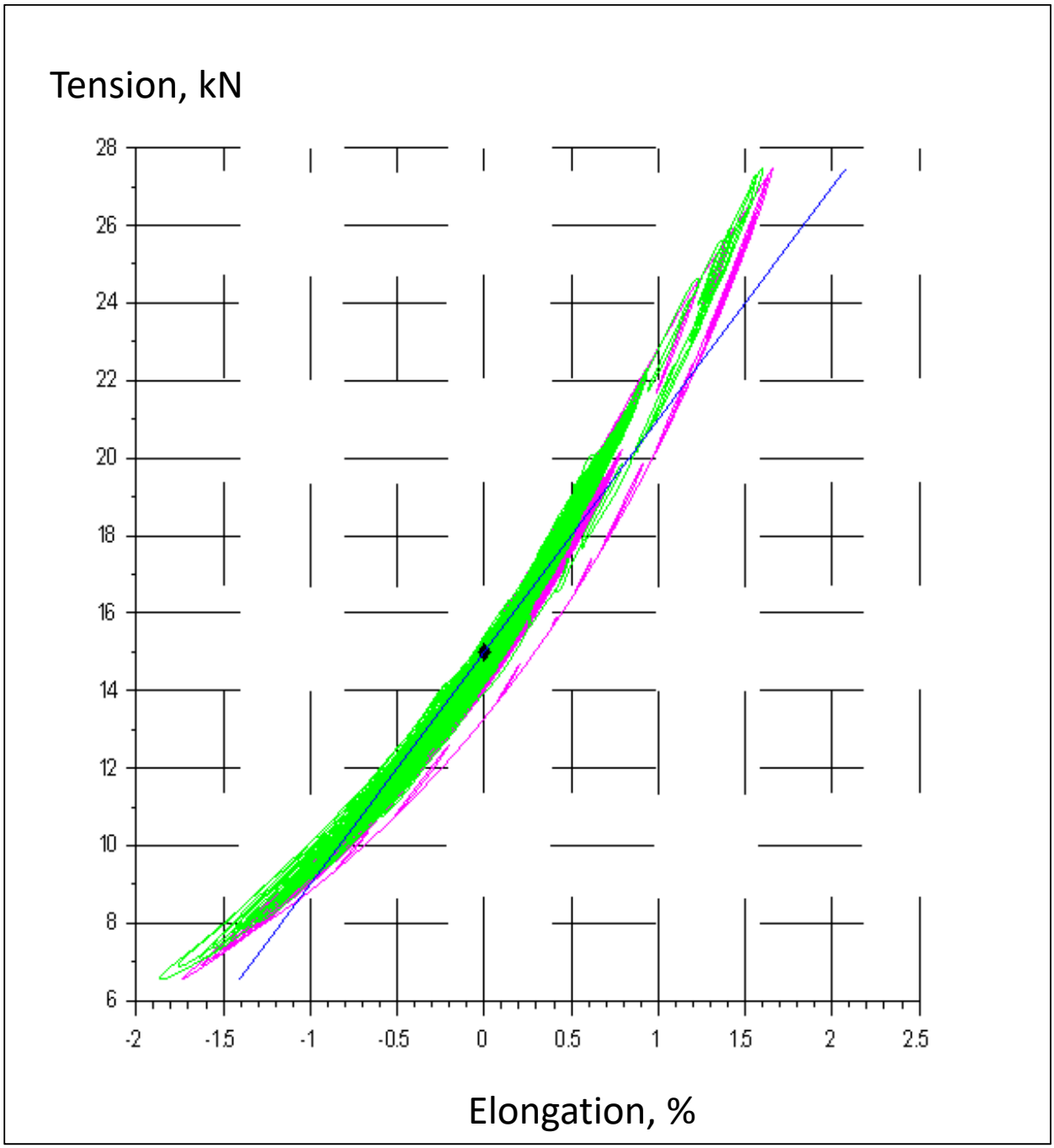

(a)

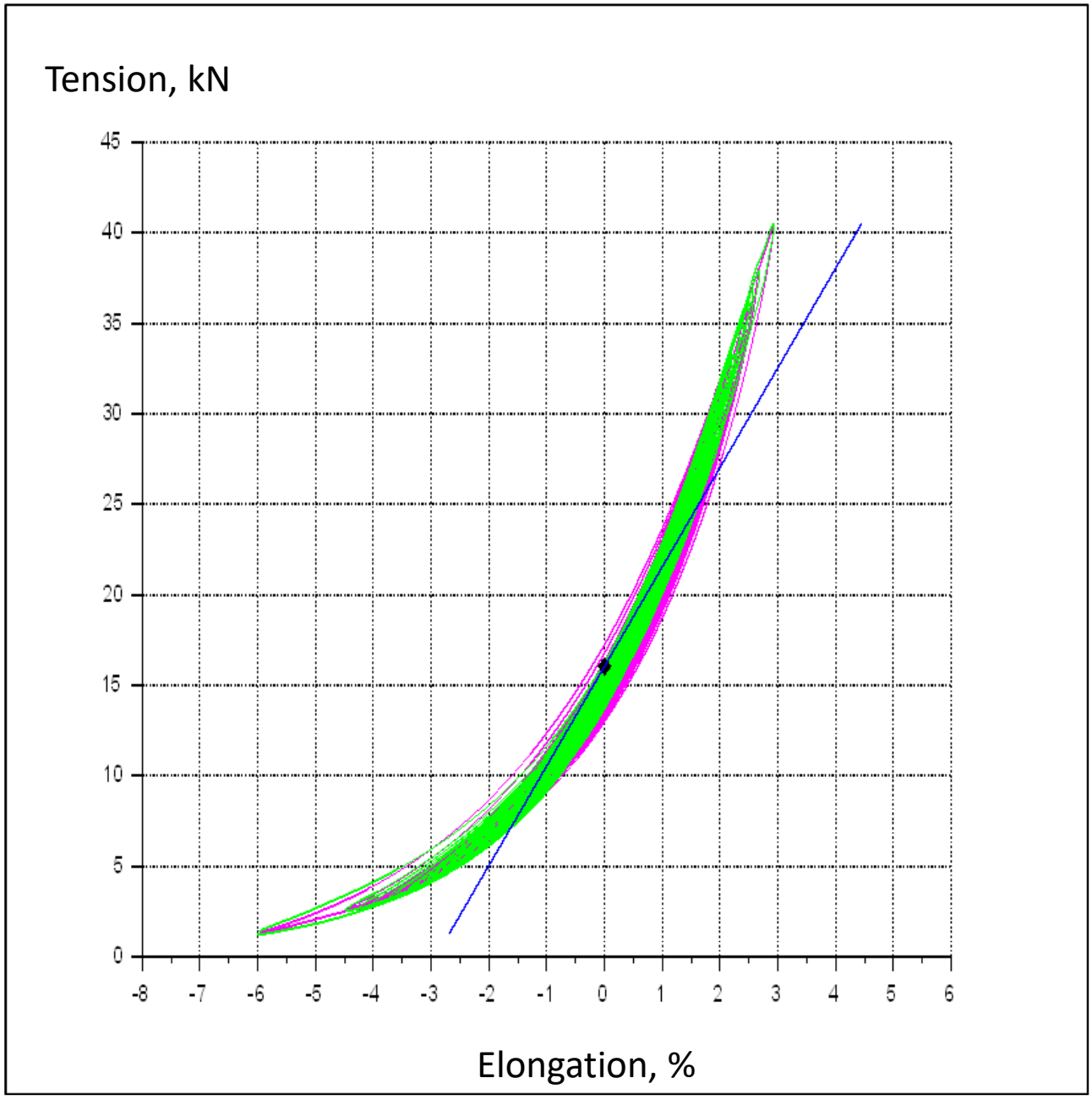

(b)

Figure 10. Tension versus elongation

(a) H32B (b) 4G

Observed (green), model (pink)

linear model (black) (see 4.4.3)

4.4 Application

With the range of tensions as noted in 2.1, this model is deemed applicable to the full range of tensions, within those allowed by mooring design codes, that may be encountered for the t design conditions (operating, fatigue, survival, …) of different types of FOWT, noting that:

> the cases of higher mean tensions (thus implying a lower range), for example in turbine operating conditions, are covered through the normalisation of tensions (see 3.3 above), and the convergence of the model towards a linear relation in such cases (see 2.3 and 3.6.3 above).

> the evaluation of near-slack conditions under a very low mean tension (leeward line), is not accurate, but this is not significant for analysis (see note at end of 3.5 above).

In mooring analyses, where the line response is driven to a large extent by the floater's imposed motions, the uncertainties on tensions (e.g. the extreme tension, and thus the required rope size) will be small.

With respect to a classical "Dynamic stiffness" model, besides resolving the designer's dilemma of amplitude dependence (a specific feature of PA, see 1.3), this model will provide a much more accurate response: The linear "stiffness" clearly underestimates maximum tension and exaggerates the occurrence of line slackening in severe storms; see 4.3 and Figure 10 above.

5 Conclusions

The lines in a station keeping system are subject to a random amplitude (stochastic) cycling. Under these conditions, the response of polyamide lines appears much more complex than that of polyester, so that they cannot be properly described, in a mooring analysis, by the now classical and (rather) simple model of a "dynamic stiffness".

In order to respond to this challenge, an empirical model was thus developed, by which a time domain evaluation of polyamide rope elongation versus applied tension can be performed.

This model was built and calibrated based on a database of rope tests under stochastic cycling, for a number of different cases, so that this model is deemed applicable to all the relevant design conditions, for different types of FOWT floaters.

It is a pseudo elastic model that reproduces the specific features of the response of fully wetted PA ropes well, with reasonable accuracy.

For the extreme (maximum and minimum) values it provides a much better prediction than the linear "dynamic stiffness" model.

This model can be integrated in the time domain processing of suitable mooring analysis software.

6 Acknowledgments

The OHP (Offshore Hawser Properties) and OHP2 JIPs (2007-2013) examined the stiffness and failure properties of polyamide hawsers for Single Point Moorings. They were sponsored by Petrobras, Total, and SBM. Their support is gratefully acknowledged.

The ANR POLYAMOOR project (2017-2020) was led by France Energies Marines (FEM) with partners Bexco, Bureau Veritas, Ensta Bretagne, Ifremer, and Naval Energies, (see https://www.france-energies-marines.org/projets/polyamoor/). It focussed on the short and long term behaviour of polyamide

The ANR MONAMOOR project (2021-2024) is also led by FEM, with partners Bexco, Bureau Veritas, CNRS, Ensta Bretagne, GeM, Ifremer, Naval Group, NCD, RWE, Total Energies, the University Gustave Eiffel, the University of Nantes and WEAMEC. This project is focussed on development of monitoring methods for polyamide mooring line integrity (see https://www.france-energies-marines.org/projets/monamoor/).

7 References

[1] Weller, S.D., Johanning, L., Davies, P., Banfield, S.J., 2015. Synthetic mooring ropes for marine renewable energy applications. Renew. Energy 83, 1268–1278. https://doi.org/10.1016/j.renene.2015.03.058

[2] Bureau Veritas (2023), Fibre ropes for offshore services, NR432

[3] International Organization for Standardization, (2018), Fibre ropes for offshore station keeping – General specification, ISO18692-1:2018

[4] Ridge, I. M. L., Banfield, S. J., & Mackay, J. Nylon fibre rope moorings for wave energy converters. In OCEANS 2010, IEEE publication.

[5] Chevillotte Y, Marco Y, Bles G, Devos K, Keryer M, Arhant M, Davies P, Fatigue of improved polyamide mooring ropes for floating wind turbines, Ocean Engineering,199, 2020,107011

[6] Civier, L., Chevillotte, Y., Bles, G., Montel, F., Davies, P., Marco, Y., 2022. Short and long term creep behaviour of polyamide ropes for mooring applications. Ocean Eng. 259, 111800. https://doi.org/10.1016/j.oceaneng.2022.111800

[7] Sørum SH, Fonseca N, Kent M, Faria RP Assessment of nylon versus polyester ropes for mooring of floating wind turbines, Ocean Engineering, 278, (2023), 114339

[8] Pham H-D, Cartraud P, Schoefs F, Soulard T, Berhault C, Dynamic modeling of nylon mooring lines for a floating wind turbine, Appl Ocean Res., (2019), 87, 1-8.

[9] Chevillotte Y. (2020). Characterization of the long-term mechanical behavior and the durability of polyamide mooring ropes for floating wind turbines. PhD Thesis, Université Bretagne Loire, ENSTA Bretagne. https://archimer.ifremer.fr/doc/00683/79537

[10] Civier L, Chevillotte Y, Bles G, Montel F, Davies P, Marco Y, Visco-elastic-plastic characterization and modelling of a wet polyamide laid-strand sub-rope for floating offshore wind turbine moorings, submitted to Ocean Engineering, January 2023.

[11] Flory, J.F., Ahjem, V., Banfield, S.J., 2007. A New Method of Testing for Change-in-Length Properties of Large Fiber-Rope Deepwater Mooring Lines, in: Proceedings OTC, Houston, Texas, U.S.A., p. OTC-18770-MS. https://doi.org/10.4043/18770-MS

[12] West W.M., Goupee, A.J., Viselli, A.M., Dagher, H.J., 2020. The influence of synthetic mooring line stiffness model type on global floating offshore wind turbine performance. J Phys Conf Ser 1452, 012044. https://doi.org/10.1088/1742-6596/1452/1/012044

[13] Xu K, Larsen K, Shao Y, Zhang M, Gao Z, Moan T, Design and comparative analysis of alternative mooring systems for floating wind turbines in shallow water with emphasis on ultimate limit state design, Ocean Engineering, 219, (2021),108377

[14] Falkenberg E, Åhjem V, Yang L, Best Practice for Analysis of Polyester Rope Mooring Systems, Paper presented at the Offshore Technology Conference, Houston, Texas, USA, May 2017. doi: https://doi.org/10.4043/27761-MS

[15] Pillai AC, Gordelier TJ, Thies PR, Cuthill D, Johanning L, Anchor loads for shallow water mooring of a 15 MW floating wind turbine—Part II: Synthetic and novel mooring systems,
Ocean Engineering, 266, 1, (2022), 112619

[16] Verde S, Lages EN, A comparison of anchor loads, planar displacement, and rotation for nylon and polyester moored systems for a 15 MW floating wind turbine in shallow water,
Ocean Engineering, 280, (2023), 114404

[17] Xu S, Guedes Soares C, Parametric study on the short-term extreme mooring tension of nylon rope for a point absorber, Ocean Engineering, 267,(2023), 113248

[18] Del Vecchio CJM, (1992), “Lightweight materials for deep water moorings”, PhD thesis University of Reading

[19] François M, Davies P et al, (2010), “Modelling fiber rope load-elongation properties - Polyester and other fibers”, Offshore Technology Conference OTC 20846

[20] François, M., Davies, P., 2008. Characterization of Polyester Mooring Lines, in: Volume 1: Offshore Technology. Proc. OMAE2008, ASME, Estoril, Portugal, pp. 169–177. https://doi.org/10.1115/OMAE2008-57136

[21] Humeau C, Davies P, Le Gac PY, Jacquemin F, 2018. Influence of water on the short and long term mechanical behaviour of polyamide 6 (nylon) fibres and yarns. Multiscale Multidiscip. Model. Exp. Des. 1, 317–327. https://doi.org/10.1007/s41939-018-0036-6

[22] Venoor V, Park JH, Kazmer D, Sobkowicz MJ, 2020, Understanding the Effect of Water in Polyamides: A Review, Polymer Reviews 61, (3)1-49, DOI: 10.1080/15583724.2020.1855196

[23] Rychlik I, 1987. A new definition of the rain flow counting method, International Journal of Fatigue, 9, pp. 119–21.

[24] SCILAB “The open source platform for numerical computation” (copyright © INRIA, ENPC)